A Study on Effect of Intergranular Corrosion by Heat Input on Inconel 625 Overlay Weld Metal

Joon-Suk Kim[1] and Hae-Woo Lee[1,]*

Department of Metallurgical Engineering, College of Engineering, Dong-A University, Busan, 604-714, Republic of Korea
[*]E-mail: hwlee@dau.ac.kr,

This study discusses the effect of welding heat input on intergranular corrosion of the weld metal of Inconel 625 alloy. A specimen of Inconel 625 overlay with a weld metal that controlled welding heat input was manufactured, and aging heat treatment was conducted to investigate sensitization by chromium carbides. The electrochemical single-loop (SL) and double-loop (DL) electrochemical potentiokinetic reactivation (EPR) experiments, together with the chemical ferric sulfate-sulfuric acid and nitric acid tests, were conducted to determine intergranular corrosion susceptibility between the specimens. In the SL and DL EPR experiments, specimens were stabilized in the weld metal, and therefore intergranular corrosion susceptibility could not be determined. However, in the ferric sulfate-sulfuric acid and nitric acid tests, the corrosion speed increased as heat input increased. This was because the amount of diluted Fe increased as the welding heat input increased, leading to microsegregation between the dendrites, which had a negative effect on the corrosion resistance.

1. INTRODUCTION

Inconel 625, which is a Ni-base alloy, is a super heat-resistant alloy that has excellent mechanical properties under high-temperature conditions and high corrosion resistance. Because of this, it has been widely used as a structural material for steam engines, nuclear power generators, and aircraft engines [1-9]. It also has superior welding characteristics, and consequently, it is used for weld overlay inside carbon steel pipes [10-12]. Thus, it can replace existing high corrosion-resistant steels such as duplex stainless steels, for use in offshore plants. Weld overlay cladding steel has economic advantages over duplex stainless steel. It can also have a synergistic effect, by weld overlay with carbon steel materials, to complement the relatively low yield strength of Inconel alloy and low

corrosion resistance of carbon steel; therefore, it can be used as structural materials in highly corrosive environments, such as those in the presence of crude oil. In addition, the thermal expansion coefficients of the two metals are similar, which reduces the possibility of cracks due to thermal stress under high-temperature conditions [13-15]. However, the Inconel alloy consists mainly of Ni and Cr, which may generate carbides and secondary phases, depending on the specific temperature and exposure time. These carbides and secondary phases play a role in the degradation of the corrosion resistance and physical properties of the alloys and lead to the formation of crack points [16, 17]. As can be seen from the TTT(Time-Temperature Transformation) curve of Inconel 625 alloy, various carbides and secondary phases are formed over time, including MC, $M_{23}C_6$, M_6C, γ'', and the Laves phase [18]. γ'' is tetragonal Ni_3Nb, which precipitates in the temperature range of 600–750℃. $M_{23}C_6$ (M : Cr, Mo) precipitates at temperatures of 750–950℃, and has the composition ratio of Cr 70%, Ni 26%, and Fe 4%. Its size is 0.1–0.2 μm, and it has an intergranular polygonal form. M_6C (M : Mo, Nb, Cr, Si) precipitates in the temperature range of 800–1050℃ and contains 96% or more Cr. Its size is 1–1.5 μm, and it is produced in an intergranular pseudo-hexagonal form. MC (M : Nb, Ti, Mo) is formed in the temperature range of 800–1000℃ [19]. γ'' and Laves phases are generated when kept in an isothermal environment for long times and are produced by transformation of carbides. The formation of such carbides can be a factor contributing to the degradation of corrosion resistance. Intergranular areas of carbides are thermodynamically more unstable and react more readily than other intragranular ones. Intergranular areas increase owing to the formation of carbides. Furthermore, the carbides have a higher Cr concentration than that in the base metal. Thus, when carbides are formed in intergranular areas, the Cr concentration around them decreases, and as a result, Cr deficient areas are formed along the intergranular region. This phenomenon, in which Cr deficient areas are more susceptible to intergranular corrosion than other areas, thereby initiating corrosion, is called sensitization [20].
 This study aims to identify the effect of welding conditions on the carbide precipitation tendency and intergranular corrosion. Specimens where welding heat inputs were controlled were submitted to aging heat treatment to precipitate carbides, and the susceptibility of intergranular corrosion of different specimens was compared through intergranular corrosion experiments. The cause of differences between them was analyzed.

2. EXPERIMENTAL PROCEDURES

2.1. Specimen preparation

This study used the electroslag welding (ESW) method, with the Inconel alloy, EQNiCrMo-3, used as the filler metal. This is specified in the ASME, and the flux used for weld overlay was SA FB 2 Cr Mo Nb, specified in EN 760. The shape of the weld metal is shown in Fig. 1. The welding conditions of specimens used in this study are given in Table 1, which lists the characteristics according to the welding heat input. Amperage was controlled, while voltage and speed were kept constant to control welding heat input. Table 2 shows the composition of the Inconel strip, and carbon steel, taken as the base metal. Table 3 shows the composition of the weld metal where ESW was

performed, using the conditions given in Table 1. The composition ratio was measured using a Spark Emission spectrometer.
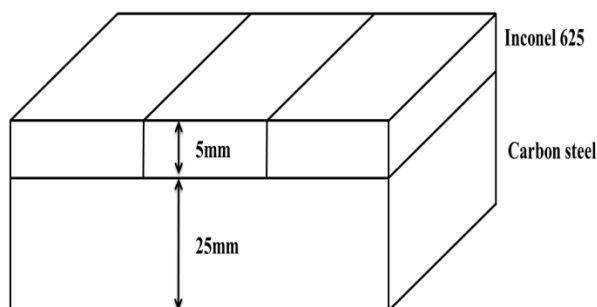

Figure 1. The schematic of the weld metal

Table 1. Welding parameters.

No.	Filler Metal Size	Polarity	Amperage	Voltage	Speed (cm/min)	Max.Heat Input (KJ/cm)
500A			500			43.3
570A	0.5T * 30W	DCRP	570	26	18	49.4
620A			620			53.7

Table 2. Composition of filler and base metal.

	C	Mn	Si	Cr	Ni	Mo	Nb	Fe	Ti
Inconel Strip	0.015	0.1	0.1	22	Bal	9	3.6	0.3	0.23
Base metal	0.47	0.68	0.20	0.08	0.07	0.02	0.004	98.2	0.01

Table 3. Composition of specimens.

	C	Mn	Si	Cr	Ni	Mo	Nb	Fe	Ti
500A	0.013 ~0.015	0.051 ~0.055	0.32 ~0.34	20.56 ~20.60	62.21 ~62.45	8.45 ~8.58	3.40 ~3.51	4.50 ~4.62	0.036 ~0.039
570A	0.013 ~0.016	0.047 ~0.050	0.31 ~0.37	21.04 ~21.41	62.64 ~62.88	8.37 ~8.46	3.34 ~3.57	4.49 ~4.79	0.037 ~0.040
620A	0.014 ~0.016	0.043 ~0.051	0.28 ~0.35	21.21 ~21.73	62.37 ~62.56	8.76 ~8.90	3.55 ~3.79	4.63 ~4.90	0.040 ~0.042

2.2. Aging heat treatment

Aging heat treatment was conducted to determine the intergranular corrosion resistance of 500A, 570A, and 620A specimens under as-weld conditions. Based on the TTT curve of Inconel 625 alloy given in Fig. 2, isothermal aging heat treatment was conducted to form chromium carbides. Heat treatment was conducted in an air atmosphere for 100 h, using a vertical tubular furnace at a temperature of 850°C, thereby manufacturing specimens of AT-500A, AT-570A, and AT-620A. As a consequence of this isothermal aging heat treatment, $M_{23}C_6$ and M_6C precipitation was induced to form a Cr deficient area.
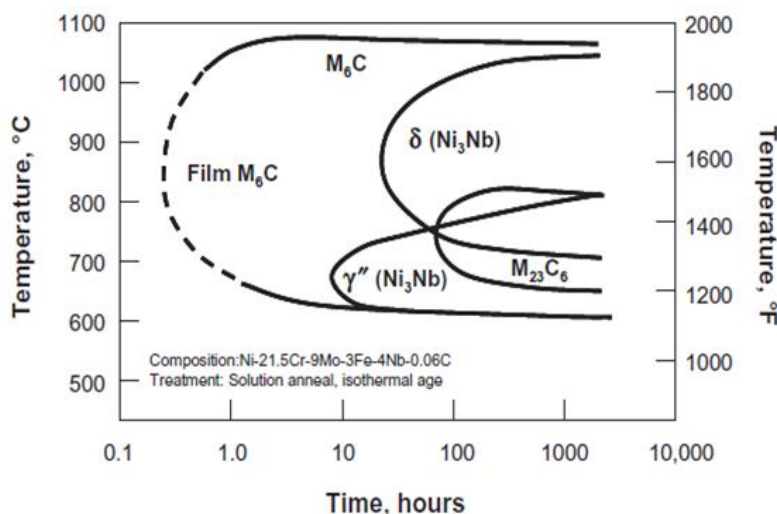

Figure 2. TTT curve of Inconel 625 alloy

2.3. Corrosion experiments

A single-loop and double-loop electrochemical potentiokinetic reactivation test (SL and DL EPR test) was conducted as an electrochemical method to judge the intergranular corrosion resistance. This test is less destructive and more quantitative than chemical ones. Duffaut et al. have measured the susceptibility of intergranular corrosion of Inconel alloys quantitatively based on the results of studies by Edeleanu and Prazak [21] and Novak et al. [22], who developed this method. The EPR method has two types of tests: single loop and double loop ones. In the single loop test, the errors observed can be high if uneven corrosion occurs in the intergranular area, and the results should be calculated using the current ratio or charge ratio. In contrast, in the double loop test, errors due to surface conditions are small and the experimental values can be easily obtained, and compared with those of the single loop test. Maday et al. [23] reported that the double loop test made it easier to identify intergranular corrosion than the single loop test. EPR test condition parameters of Ni-based alloy were reported in previous studies. Maday et al. [23] reported that when the concentration of H_2SO_4 was high, both intergranular corrosion and other types of corrosion progressed, whereas intergranular corrosion was not observed if its concentration was low. Thus, based on the test condition parameters used in previous work, this study conducted experiments applying these to Ni-based alloy. The detailed

experiment conditions are summarized in Table 4. Q values, which the area between activation peak and curve, among specimens were compared with polarization curves obtained through the SL EPR test, while the I_r value, i.e., the maximum anodic current density, and I_a value, i.e., the maximum reactivation current density, were obtained via the DL test. Finally, these allowed the calculation of the Dos value I_r/I_a to evaluate the intergranular corrosion susceptibility. The corrosion cell used in the DL EPR test comprised Ag.Agcl/KCl(sat'd) as the reference electrode and platinum foil as the counter electrode.

Table 4. Corrosion ratio after intergranular chemical Test.

	Corrosion area
AT-500A	0.65%
AT-570A	1.27%
AT-620A	1.52%

In the chemical test method to measure intergranular corrosion of stainless steel or Ni-based super alloy, the ferric sulfate-sulfuric acid and nitric acid tests were conducted. The ferric sulfate-sulfuric acid test is specified in the ASTM G28 Method A as a method to measure intergranular corrosion susceptibility of Ni-based or Cr bearing alloys [24]. For the ferric sulfate-sulfuric acid solution, a sulfuric acid solution containing 400 ml H_2O and 236 ml H_2SO_4, in which 25 g $Fe_2(SO_4)_3$ was dissolved, was used. This solution was heated on a hot plate, the specimen was immersed for approximately 120 h, and weight loss was measured. To prevent evaporation of the solution over 120 h, a boiling stone was placed in the solution, and the solution vapor was condensed using a flowing water condenser. The experimental results were obtained by substituting the observed weight loss of the specimens into the corrosion speed equation specified in Section ASTM G28 8.1, which compares corrosion rate between specimens [24]. Another chemical test, the nitric acid test, was conducted in accordance with ASTM A262 Method C [25]. However, this method was designed for optimization for austenitic stainless steel, and so was modified to suit the Ni-based alloys used in this study. Because the PREN index of Ni-based alloys was higher than that of austenitic stainless steel, the immersion time was increased from the suggested 48 h to 120 h in this experiment. The experimental procedure and data analysis were similar to those in the ferric sulfate-sulfuric acid test, except for replacing the reaction medium with 65% nitric acid solution.

3. RESULTS AND DISCUSSION

Fig. 3-(a) shows the experimental results for AT-500A, AT-570A, and AT-620A obtained after the SL-EPR test. The three curves had a similar shape. A common passive region was observed from 0

to 1 V, and the Q value region occurred in the zone that determines the level of intergranular corrosion. Comparison of the results for the Q values among specimens showed no significant differences. Similar behavior was seen with DL-EPR. Fig. 3-(b) shows the DL-EPR test results for AT-500A, AT-570A, and AT-620A. Although, strictly, the Dos value, I_r/I_a, should be compared, the I_r value was not found for all the three curves, so that intergranular corrosion cannot be determined with only the Dos value. From the SL and DL EPR test, no intergranular corrosion was observed between specimens. This is due to the fact that the carbon content in Inconel 625 alloy was minimal, whereas the Nb content was large. Because of the low carbon content, chromium carbides, the main cause of Cr deficient areas, were not precipitated during aging heat treatment, and thanks to the Nb effect, Nb carbides precipitated, thereby inhibiting chromium carbide generation. Fig. 4 shows the SEM image of the Nb carbides, indicating the specimen stabilization resulting from precipitation along the grain.
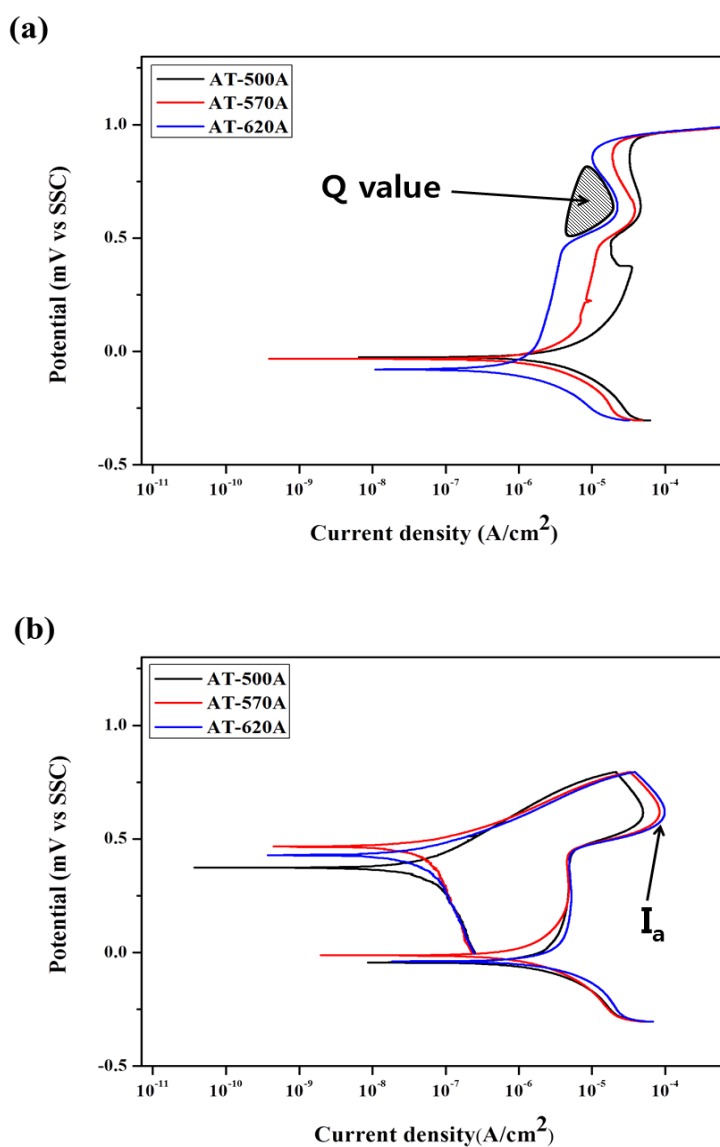

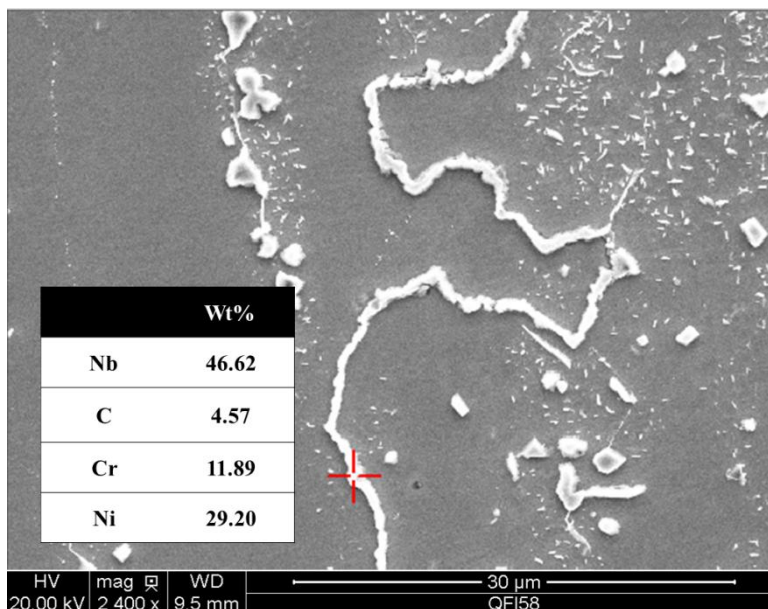**Figure 3.** The experimental results for the (a) SL-EPR test and (b) DL-EPR test

Figure 4. The SEM image of the Nb carbides, indicating the specimen stabilization resulting from precipitation along the grain.

Table 5 shows the data from the ferric sulfate-sulfuric acid and nitric acid tests. The results of substituting them into the corrosion rate equation (specified in Section ASTM G28 8.1) are shown in Fig. 5. As can be seen from Table 5, the results of the two tests indicate a tendency of an increasing weight loss as the heat input of the specimen increased, as is observed for AT-500A to AT-620A. The varying parameters in the corrosion rate equation, specified in Section ASTM G28 8.1, are weight loss and specimen area, while other factors are the same. Since the specimen was manufactured as close to the same size as possible, the weight loss was main variable, such that AT-620A showed the fastest corrosion rate because it had the largest weight loss.

Table 5. Result of Ferric sulfate sulfuric & Nitric acid Test.

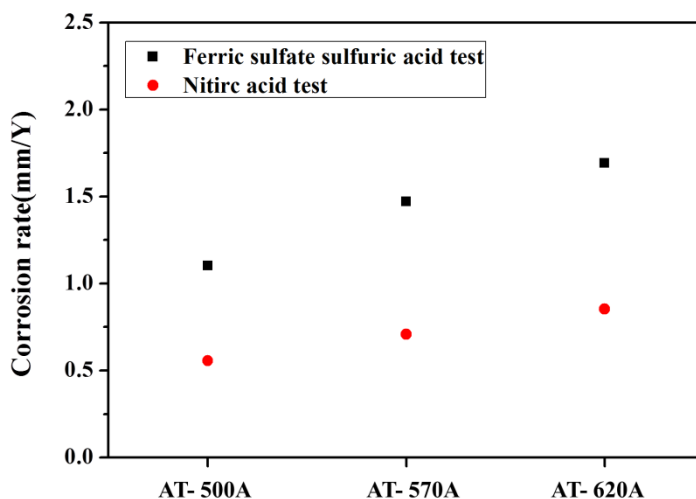|	Specimen	K (constant)	W(Weight loss, g)	A(area, cm^2)	T (Time, T)	D(density, g/cm^3)
Ferric Sulfate sulfuric acid	No.4		0.0406	3.185		
	No.5	$8.76*10^4$	0.0574	3.376	120	8.44
	No.6		0.0646	3.304		
Nitric acid	No.4		0.0205	3.458		
	No.5	$8.76*10^4$	0.0261	3.506	120	8.44
	No.6		0.0315	3.487		

Figure 5. The results of substituting them into the corrosion rate equation

The reason for the different corrosion rates was due to the corrosion type. To analyze this, microstructures of the corrosive surfaces were observed after the two chemical tests with SEM. Fig. 6 shows high magnification SEM images of AT-500A, AT-570A, and AT-620A after the ferric sulfate-sulfuric acid test. The white region shows a dendritic structure. Since specimens were cut vertically in the direction of dendritic growth, the dendritic nucleus and interdendritic area were observed. All specimens experienced corrosion initially at the intersection between intergranular and dendritic areas. The corrosion tendency showed that as the progression was made from AT-500A to AT-620A, the corrosive regions became larger. In AT-500A, a thin and long corrosion shape was found, while in AT-570A, this corrosion region had grown further. In AT-620A, the corrosion region progressed circularly. This was because as heat input increased, carbides grew gradually, thereby increasing the corrosion rate. Fig. 7 shows areas where corrosion occurred in AT-500A, AT-570A, and AT-620A after the ferric sulfate-sulfuric acid test, while Table 5 presents the corresponding numerical values.
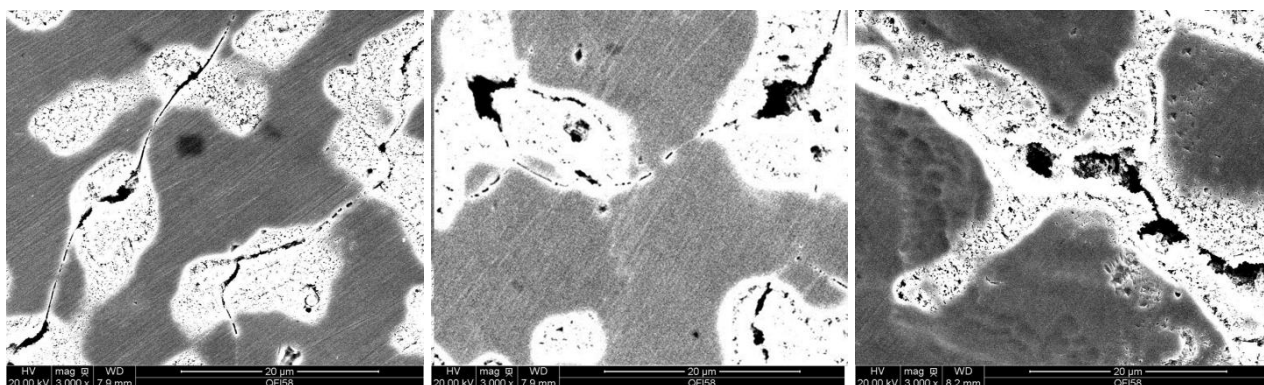

Figure 6. The high magnification SEM images of (a) AT-500A, (b) AT-570A, and (c) AT-620A after the ferric sulfate-sulfuric acid test.
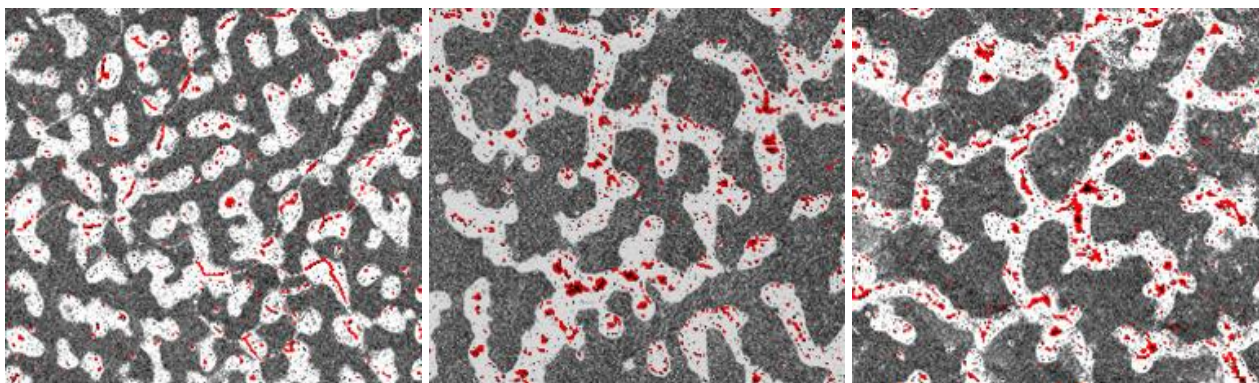
Figure 7. The areas where corrosion occurred in (a) AT-500A, (b) AT-570A, and (c) AT-620A after the ferric sulfate-sulfuric acid test.

Results comparing the corrosion part (red colored region) with the total area using the same magnification showed that AT-620A had the largest corrosion region. Similar results were obtained in the ferric sulfate-sulfuric acid test.

The corrosion growth with increasing welding heat input is due to Fe dilution occurring in the fusion line. In general, the larger the welding heat input, the more dilution occurs in the weld metal and base metal. According to work by Kumar et al. [26], when welding heat input increases, a part of base metal is melted, so that atoms in the base metal are diluted into the weld metal. This results in an increase in diluted Fe content in the weld metal, thereby reducing the breakdown potential. Such Fe dilution phenomena have also been observed previously in the melted zone and can be observed in the fusion line zones through energy dispersive X-ray spectroscopy (EDS) measurements. Fig. 8 shows the SEM image observed around the fusion line.
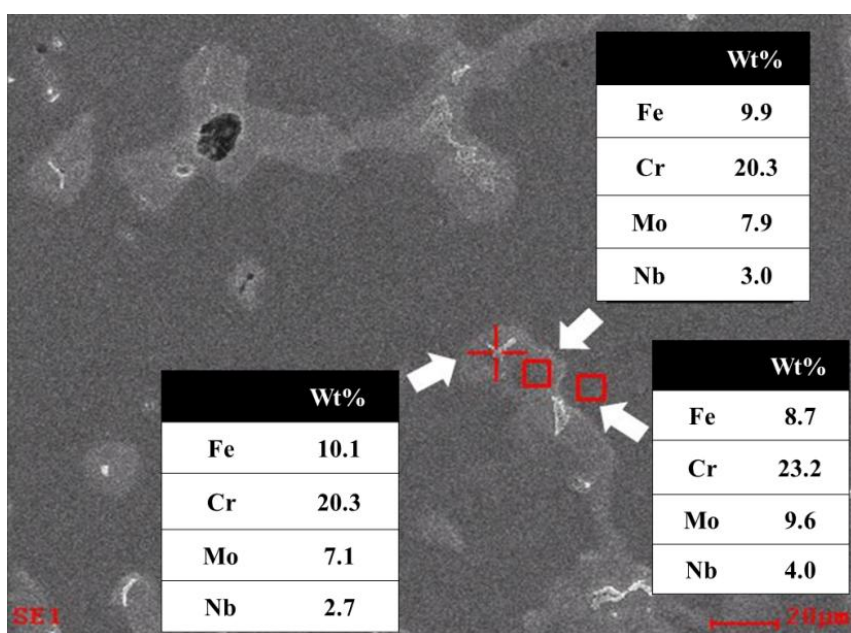

Figure 8. The SEM image observed around the fusion line

The EDS measurements of changes in composition in the interdendritic area and dendritic nucleus showed a higher Fe content than that measured in Table 3. Furthermore, Cortial et al. [27] reported that high contents of Ni and Fe were observed in dendritic areas, while high contents of Nb and Mo were observed in interdendritic areas, thereby causing segregation. Such segregation was due to the release of Nb and Mo from the dendritic nucleus upon weld solidification. Thus, as heat input increased, the dilution effect increased, thereby increasing the Fe content in the fusion line. Consequently, a large amount of Fe was coagulated, first in dendritic areas, upon weld solidification and Nb and Mo were released into interdendritic areas. Such phenomena induced microsegregation in dendritic and interdendritic areas, thereby creating a difference in corrosion resistance between two regions, resulting in a difference in corrosion shape. The results of the measured composition inside the dendritic and interdendritic areas, shown in Fig. 6 using EDS, are presented in Table 6. The largest microsegregation was observed in AT-620A.

Table 6. Composition of dendrites and spaces.

Chemical element	No.4			No.5			No.6		
	Dendrites	**Spaces**	**Gap**	**Dendrites**	**Spaces**	**Gap**	**Dendrites**	**Spaces**	**Gap**
Ni	62.2	61.7	0.5	63.6	61.1	2.5	64.2	60.5	3.7
Fe	6.6	5.6	1.0	8.4	7.1	1.3	10.1	8.7	1.4
Cr	20.7	21.5	0.5	20.6	21.7	1.1	20.3	23.2	2.9
Mo	8.0	8.7	0.7	7.8	9.1	1.3	7.1	9.6	2.5
Nb	3.1	3.1	0	2.9	3.5	0.6	2.7	4.0	1.3

4. CONCLUSION

In this study, the following results were obtained on the effect of welding heat input on intergranular corrosion susceptibility in the Inconel 625 overlay weld metal.

- Results of the electrochemical SL and DL EPR test for AT-500A, AT-570A, and AT-620A showed that the three curves had similar shapes. Furthermore, in the SL EPR test, no significant difference in Q values was found, while in the DL EPR test, no I_r was found. Thus, intergranular corrosion susceptibility between specimens was not determined. Despite nitrogen aging heat treatment, the chromium carbide did not precipitate, and the stabilization induced by the Nb carbide effect, .

- The results of the ferric sulfate-sulfuric acid and nitric acid tests, which are chemical tests, showed that as heat input increased, the weight loss increased, thereby increasing the corrosion rate. The effects on the increase in corrosion rate were because of gradual changes in corrosion growth shape from planar to spherical as heat input increased.

- The growth of corrosion shape with the increase in welding heat input was due to the effect of microsegregation caused by Fe dilution of base metal. As the heat input increased, Fe of base metal was diluted into a weld metal, where it coagulated, initially into a dendritic area, upon weld solidification, thereby releasing Nb and Mo into the interdendritic area. Such differences in anti-

corrosion atom contents between dendritic and interdendritic areas were observed as microsegregation, thereby affecting corrosion resistance negatively.

References

1. W.F. Smith, Mcgraw-Hill, *Structure and Properties of Engineering Alloy*, Technology & Engineering (1981)
2. *Corrosion of Nickel Base Alloys*, ASM International, Metals Handbook, 9th Ed., (1987)
3. G.P. Airey, *Metallography,* 13 (1980) 21–41
4. R.A Page and A. Mcminn, *Metall. Trans. A,* 17 (1986) 877–887
5. J. J. Kai, G. P. Yu, C. H. Tsai, M. N. Liu, and S. C. Yao, *Metall. Trans. A,* 20 (1989) 2057–2067
6. K. S. Kim, H. J. Lee, B. S. Lee, I. C. Jung, and K. S. Park, *Nucl. Eng. Des,* 239 (2009) 2771–2777
7. H. Xue, Z. Li, Z. Lu, and T. Shoji, *Nucl. Eng. Des,* 241 (2011) 731–738
8. K. Shinozaki, *Journal of the Japan Welding Society,* 69 (2000) 447–464
9. W. Wu and C.H. Tsai, *Metall. Trans A*, 30 (1999) 417–426
10. L. Jian, C.Y. Yuh, and M. Farooque, *Corros. Sci,* 42 (2000) 1573–1585
11. M.D. Mathew, P. Parameswaran, and K. BhanuSankaraRao, *Mater. Charact,* 59 (2008) 508–513
12. D.E. Jordan, *Weld World,* 4 (1998) 1–9
13. O.H. Madsen, New technologies for waste to energy plants, 4th Int. Symp. on Waste Treatment Technologies, 1–12, Sheffield (2003)
14. S.K. Rai, A. Kumar, V. Shankar, T. Jayakumar, K.B.S. Rao, and B. Raj, *Scripta Mater,* 51 (2004) 59–63
15. Y. H. Lee and I. S. Kim, *Wear,* 253 (2002) 438–447
16. C. Thomas and P. Tait, *Int. J. Pressure Vessel Piping,* 59 (1994) 41–49
17. G.E. Prasad and M.K. Asundi, *Trans. Indian Inst. Metals,* 42 (1989) 291–298
18. J.B. Singh, A. Verma, B. Paul, and J.K. Chakravartty, *Engineering Failure Analysis,* 32 (2013) 236–247
19. C.V. Loier and F. Cortial, Superalloys 718, 625, 706 and various derivatives , TMS, USA (1991)
20. J. Hong, D. Han, H. Tan, J. Li, and Y. Jiang, *Corros. Sci,* 68 (2013) 249–255
21. J.C. Charbonnier and T. Jossic, *Corros. Sci,* 23 (1983) 1191–1206
22. P. Novak, R. Stefec, and F. Franz, *Corrosion,* 31 (1975) 344–347
23. M.F Maday, A Mignone, and M Vittori, *Corros. Sci,* 28 (1988) 887–900
24. ASTM Standard G28-02, Standard Test Methods for Detecting Susceptibility to Intergranular Corrosion in Wrought, Nickel-Rich, Chromium-Bearing Alloys, ASTM, Philadelphia (2008)
25. ASTM Standard A262-10, Standard Practices for Detecting Susceptibility to Intergranular Attack in Austenitic Stainless Steels, ASTM, Philadelphia (2008)
26. V. Kumar, C. Lee, G. Verharghe, and S. Raghunathan, CRA weld overlay – influence of welding process and parameters on dilution and corrosion resistance, TWI (2013)
27. F. Cortial, J.M. Corrieu, and C.V. Loier, Superalloys 718, 625, 706 and various derivatives(E.A. Loria), TMS, USA(1994).